Supplementary Information: Anisotropic Hollow Microgels that can adapt their Size, Shape and Softness

Anne C. Nickel,[†] Andrea Scotti,[*,†] Judith E. Houston,[‡,¶] Thiago Ito,[§] Jérôme Crassous,[†] Jan Skov Pedersen,[‖] and Walter Richtering[*,†,⊥]

†*Institute of Physical Chemistry, RWTH Aachen University, 52056 Aachen, Germany*

‡*Jülich Centre for Neutron Science (JCNS) at Heinz Maier-Leibnitz Zentrum (MLZ), Forschungszentrum Jülich GmbH, Lichtenbergstr. 1, 85748 Garching, Germany*

¶*European Spallation Source ERIC, Box 176, SE-221 00 Lund, Sweden*

§*Physical Chemistry, Department of Chemistry, Lund University, SE-221 00 Lund, Sweden*

‖*Department of Chemistry and Interdisciplinary Nanoscience Centre (iNANO), University of Aarhus, Gustav Wieds Vej 14, DK-8000 Aarhus C, Denmark*

⊥*JARA-SOFT, 52056 Aachen, Germany*

E-mail: andrea.scotti@rwth-aachen.de; richtering@rwth-aachen.de

Experimental Section

Synthesis

The microgel shell syntheses were done under the same amount of water but with different amount of monomers. The reaction conditions are described in the main text and the used weights of each chemical for the synthesis of each system are listed in Table S1.

Table S1: Amount of chemicals used for the small and large shell syntheses.

	HSiM40	*HSiM76*
NIPAm [mg]	396	785
BIS [mg]	26.2	52.8
MRB [mg]	0.70	1.5
KPS [mg]	26.6	54
Water [mL]	170	170

Small-angle X-Ray scattering

Small-angle X-ray scattering (SAXS) curves have been measured using the cSAXS instrument at the Swiss Light Source, Paul Scherrer Institut (Villigen, Switzerland). X-ray with a wavelength $\lambda = 0.143$ nm and a spread $\Delta\lambda/\lambda = 0.02$ % were used. A sample-detector distance of 7.12 m was used to cover the q-range of interest. The collimated beam illuminates an area of about 200×200 μm of the 2D detector with a pixel size of 172 μm and 1475×1679 pixels.

Characterization of the elliptical core

To obtain information about the core dimensions, small-angle X-ray scattering was used. The inorganic elliptical cores were measured after etching away the inner hematite. Hence, only the silica shell has to be considered, simplifying the fitting process as the inner part of the core can be set to the same contrast as the solvent. The fitting was done with the core-shell ellipsoidal model implemented in SASView[1] and the data including the fit are shown in Figure S1.The fitting of the SAXS data shows a polydispersity of about 10 % which is included in the illustrated fit. The dimensions obtained from these fits were: (330±12) nm for the major axes and (75±8) nm for the minor axes. These sizes are in good agreement with the values resulting from the analysis of the hematite silica core with TEM (see Table S2). Hence, the values obtained from SAXS are used as inner dimensions to fit the SANS data for the microgel shells with matched silica core.

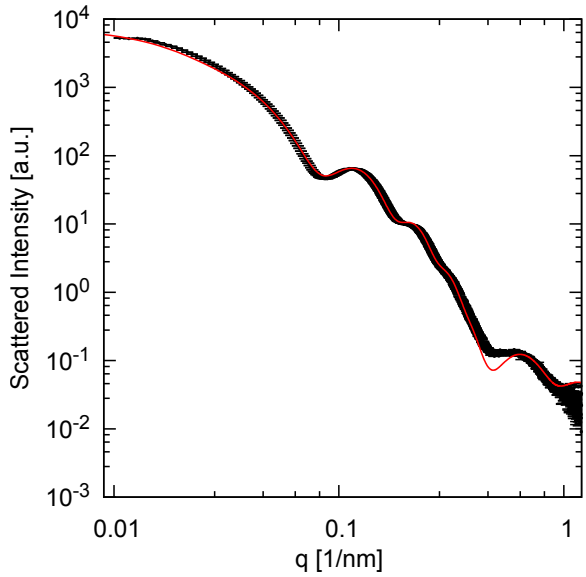

Figure S1: SAXS data of the hollow silica core dissolved in H_2O fitted with an ellipsoidal core-shell model.

Table S2: Comparison between the results of TEM and SAXS on length (L) and diameter (d) for the core.

	L[nm]	d[nm]
SAXS	330±12	75±8
TEM	284±38	81±8

Fits with spherical model

This section shows the comparison between the fits of the fuzzy spherical in *FitIt!*[2] and the fuzzy anisotropic model. This is an important step to justify the usage of more complex models instead of the simplest shape, namely the spherical shape. Hence, we demonstrate the importance of using anisotropic models to fit the scattering data adequately. Figure S2 and Figure S3 show the comparison between the fuzzy spherical model (red dashed line) and fuzzy hollow spherical model (green dashed line) fits for the best fit for, respectively, the fuzzy hollow ellipsoid or the fuzzy hollow cylinder model (solid lines, colors are chosen to match with the ones in the main text).

In Figure S2, *SiM40* (first row) and *SiM76* (second row) below (left) and above (right) the

VPTT are presented each with all three fits. In all four cases, the spherical microgel model (red dashed line) fails to reproduce the data. This is reasonable as the cryo-TEM images show the silica core inside the microgel shell, which was contrast matched for SANS. Consequently, a cavity has to be considered when fitting the scattering data, making the normal fuzzy spherical model not suitable to fit the data of *SiM76* and *SiM40* at both temperatures. Due to the anisotropically shaped silica core, similar problems appear when using the fuzzy hollow spherical model (green dashed line). For *SiM40* (first row) the fits become better compared to the model without cavity, nevertheless, all features of the scattering data at low and high temperature, which can be fitted with fuzzy anisotropic models, are not reproduced with the fuzzy spherical models. As a conclusion, a more complex model is needed to fit the scattering data properly.

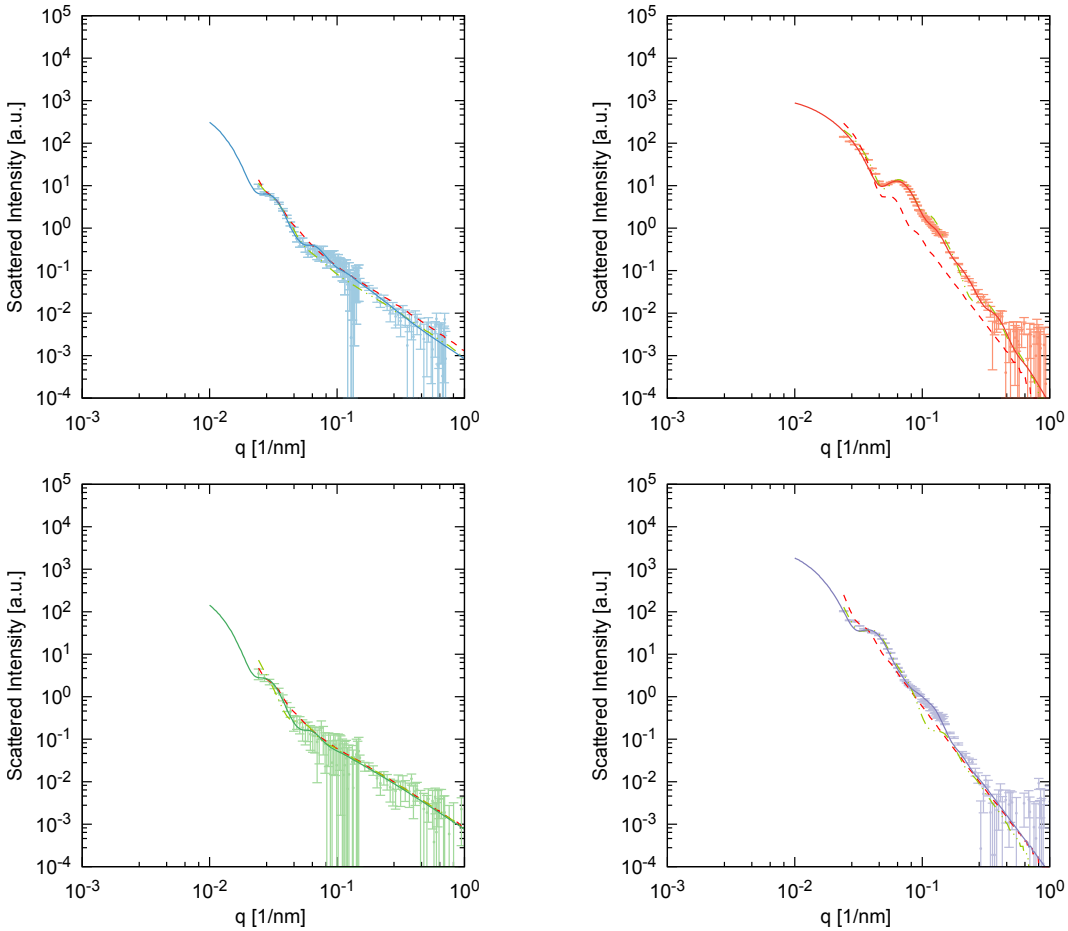

Figure S2: Spherical fits for *SiM40* (first row) and *SiM76* (second row) at 20 °C (left) and 50 °C (right). Comparison between fits for the spherical microgel (red dashed line) and hollow spherical microgel (green dashed line) models and the best fit for the anisotropic model (solid line).

The same spherical models are used to fit the data of the microgel shell only (M). The results are shown in Figure S3 in the first row for *M40* and in the second row for *M76*. Similar to Figure S2, the red dashed lines correspond to the fuzzy spherical model and the green dashed lines to the fuzzy spherical hollow model. For the hollow microgel without core the agreement between the two different spherical fits is larger compared to the *SiM* sample. When looking at *M40* for both temperatures (first row), both spherical models are able to reproduce the slope of the higher q region of the scattering data, but fail to fit the lower q region with features like shoulders and minimum. Therefore, these spherical models are not appropriate for fitting the data of *M40* at neither temperature. In comparison to that,

there is a good agreement between the fuzzy cylinder hollow model and the data (solid lines, colors are chosen to match with the ones in the main part).

In the second row of Figure S3, the data of *M76* at both temperatures are fitted with the fuzzy spherical and fuzzy spherical hollow model to compare it to the fit of the fuzzy cylinder hollow model. The plots on the left show this comparison below the VPTT at 20 °C with a good agreement between the data and both the spherical and the cylinder models. Hence, in this particular case the usage of the more complex anisotropic fits is not crucial, but still results in the best fit of the scattering data. This observation shows that the microgel with the thick shell in the collapse state has the most spherical shape of both microgels at all states. This is in agreement with the cylinder fit of *M76* at 20 °C as it has the lowest aspect ratio compared to all other states. Furthermore, as the quality of the fuzzy spherical and the fuzzy hollow spherical model fit look similar, the cavity has a minor influence for the large microgel shell. This means that the thick microgel shell has a nearly spherical shape with a small cavity in the swollen state. Compared to the fits at 20 °C, for *M76* at 50 °C above the VPTT a clear improvement when comparing the fuzzy anisotropic cylinder fit to the spherical ones is achieved. Hence, when collapsing the microgel, the shape is changing drastically and an anisotropic model is definitely required.

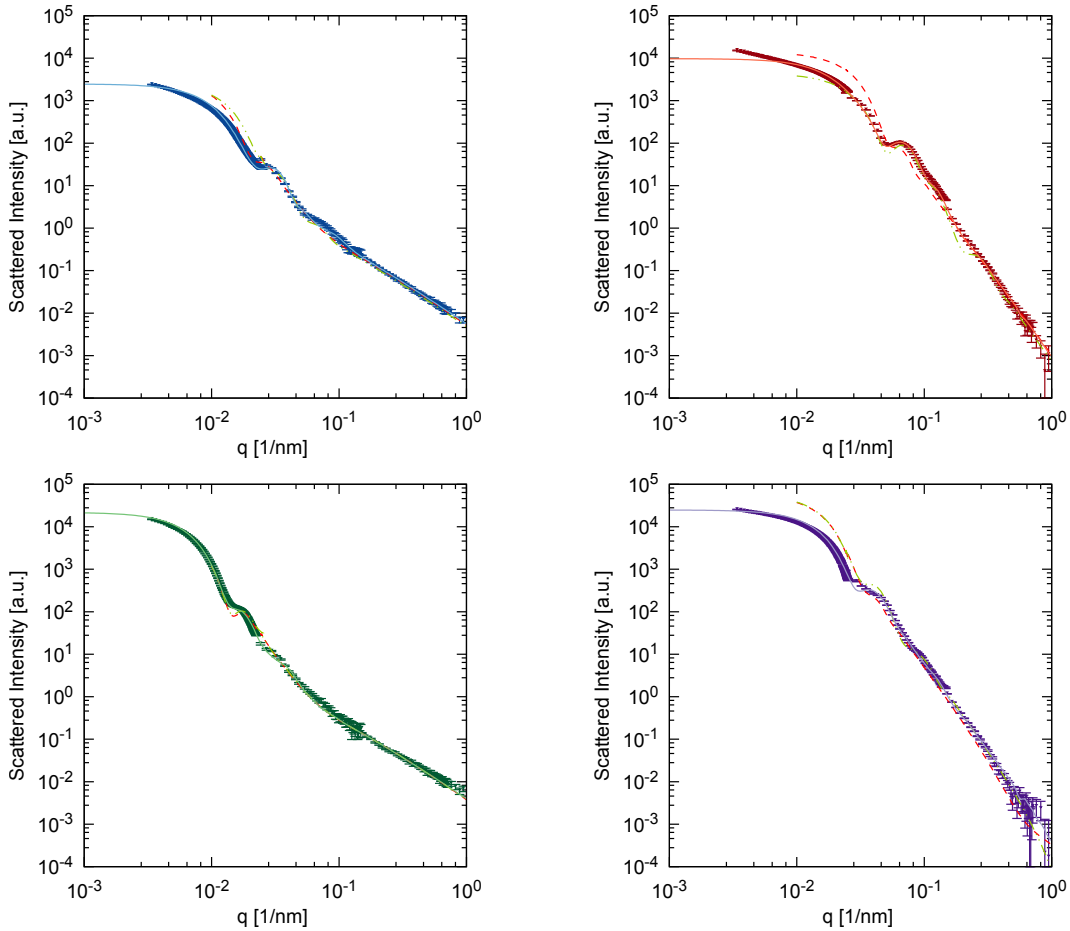

Figure S3: Fits for spherical models for *M40* (first row) and *M76* (second row) at 20 °C (left) and 50 °C (right). Comparison between fuzzy spherical (red dashed line) and fuzzy hollow spherical (green dashed line) model to the best fit for the fuzzy anisotropic model (solid line).

Concluding, the results show that neither the fuzzy spherical model nor the fuzzy spherical hollow model are suitable fitting all scattering data of the anisotropic microgels properly. As a next step, anisotropic models with sharp interfaces need to be considered for the fitting of the scattering data as they are more complicated and have more fit parameters compared to spherical ones, but less than anisotropic models with a fuzzy structure.

Fits for elliptical/cylinder models with sharp interfaces

Section presents the comparison between the "sharp-interface" and fuzzy anisotropic models used for fitting the scattering data of *SiM* and *M* for both microgels. With this comparison, we demonstrate the importance of the fuzziness to fit the data for the anisotropic microgels. In Figure S4 the scattering data for *SiM40* (first row) and *SiM76* (second row) at 20 °C (left) and 50 °C (right) are shown with the fits using sharp-interface and fuzzy ellipsoidal models. Only the ellipsoidal shape is considered as the inner dimensions are set by elliptical silica core (which is contrast matched for these data). The sharp-interface ellipsoidal model (grey solid line) is compared to the fuzzy ellipsoidal model (solid lines, colors are chosen to match with the ones in the main text).

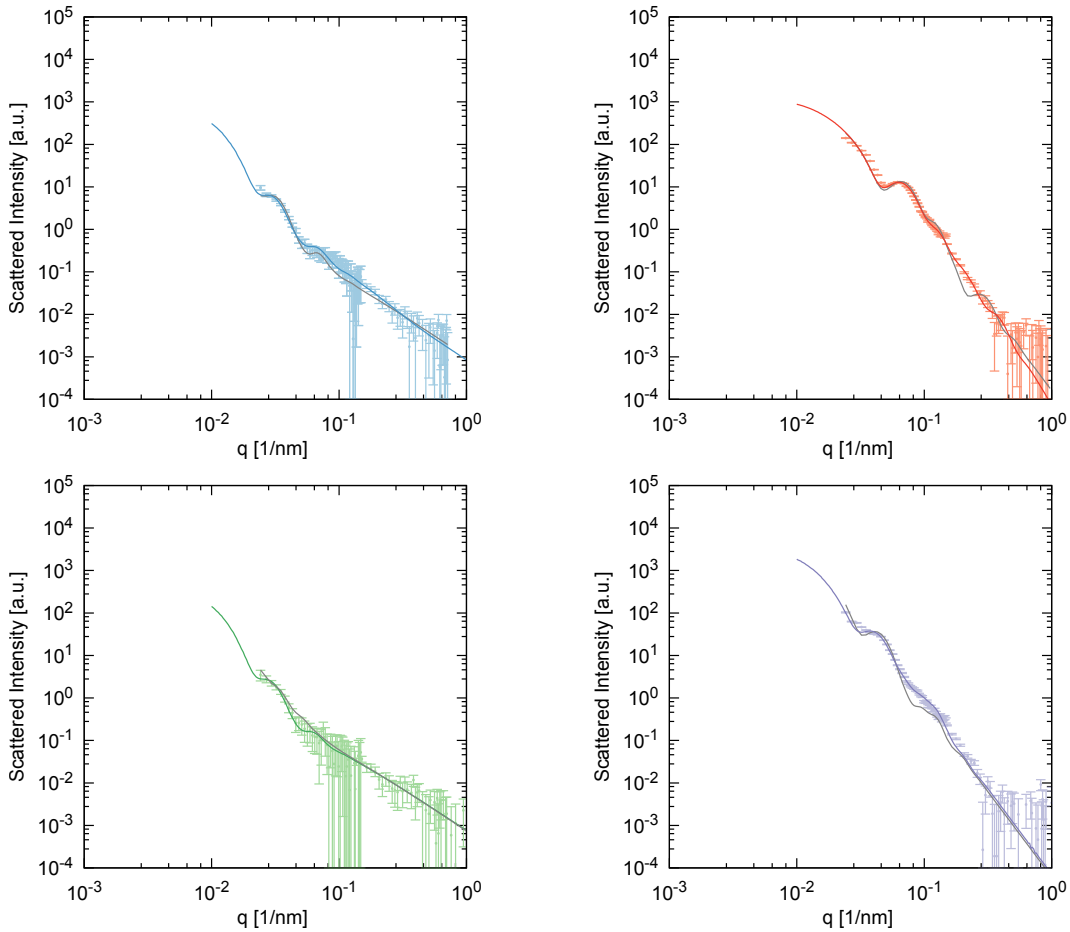

Figure S4: Sharp-interface ellipsoid model fits for *SiM40* (first row) and *SiM76* (second row) at 20 °C (left) and 50 °C (right) compared to the respective fuzzy ellipsoidal model fits.

Both microgels show a similar trend: The high-q region is fitted reasonably well with the sharp-interface model, as either the Lorentzian term is added to fit the polymer contribution in the swollen state or the slope of -4 at 50 °C in the collapsed state is fitted adequately without this addition. Nevertheless, only the fuzzy elliptical model manage to fit the mid-q range for all four stages shown in Figure S4. Hence, the fuzziness is needed to get a good agreement with the scattering data.

Figure S5 shows the comparison between the fits of the sharp-interface ellipsoidal (grey solid line) and cylinder (pink solid line) model with the best fits of the cylinder microgel model (solid lines, colors are chosen to match with the ones in the main text) for the microgels without core. *M40* is presented in the first row and *M76* in the second with the scattering data below the VPTT (left) and the scattering data above the VPTT (right), respectively. Both shapes, ellipsoid and cylinder, are used as no core is fixing the inner shape. Similar to the previous case of *SiM40* and *SiM76*, the sharp-interface models do not fit especially the mid-q regime of the microgel data *M40* and *M76* at all states. Hence, the sharp-interface models cannot characterize the fuzzy interface structure in the swollen state.

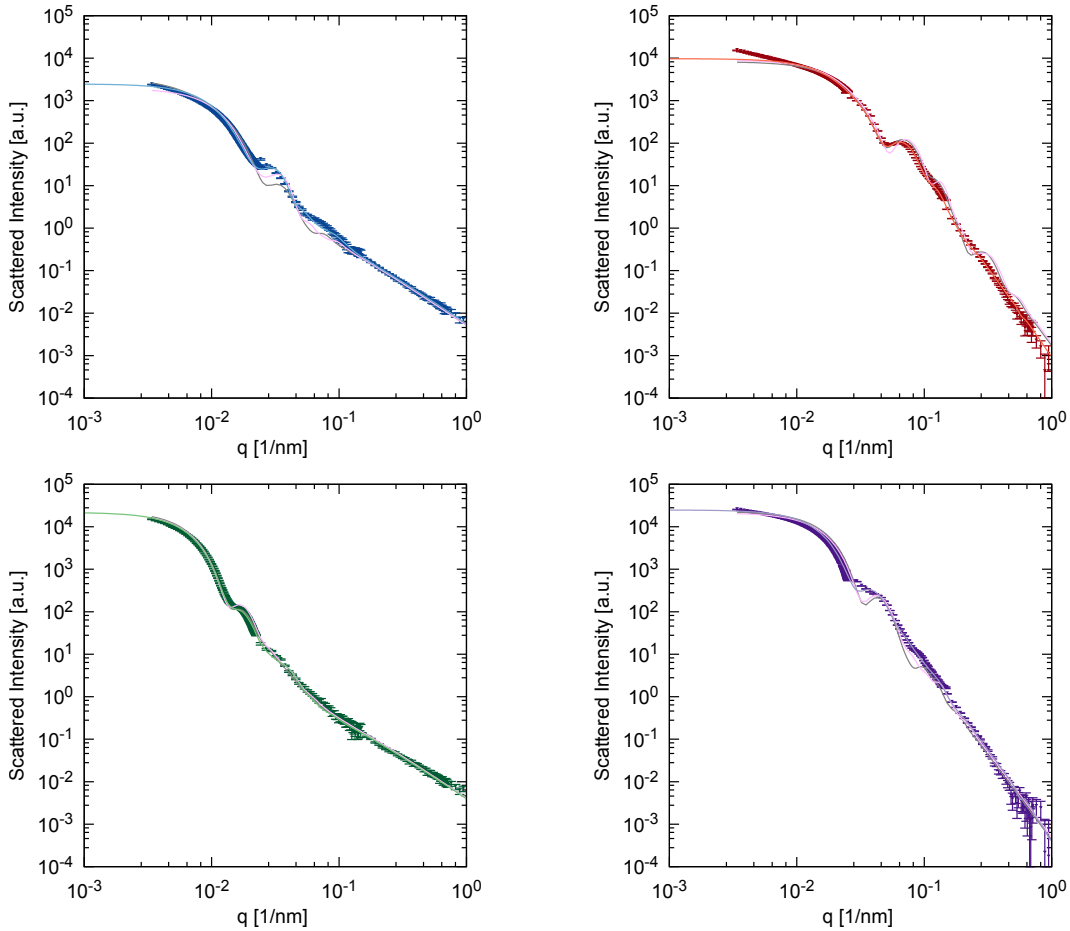

Figure S5: Sharp-interface ellipsoid model fits (grey solid line) and sharp-interface cylinder model fits (pink solid line) for *M40* (first row) and *M76* (second row) at 20 °C (left) and 50 °C (right) compared to the respective fuzzy cylinder model fits.

The data of the microgels *M40* (first row, right) and *M76* (second row, right) in the collapsed state above the VPTT indicate that the sharp-interface models are more suitable to fit the scattering data of the microgels in the collapsed state compared to the swollen one. Nevertheless, the fits of the sharp-interface models show an increase in features/minimum for both microgels compared to the fuzzy model with the same polydispersity of 13 %. Not all these features reproduce the scattering data, meaning that even in the collapsed state, the fuzzy cylinder model offers the best fit.

As a conclusion, with the existing models it was not possible to fit the scattering data of anisotropic hollow microgels in the swollen and collapsed state. Hence, we developed new

models accounting both for anisotropy and fuzziness.

Fuzzy anisotropic hollow models

Models for fuzzy anisotropic hollow microgels are developed based on the cylinder and ellipsoid shape with different polymer volume fraction profiles for the shell. As we aimed for anisotropic and hollow microgels, all models have a cavity in the inner part meaning that no polymer density/volume fraction is visible, resulting in a value of 0. Furthermore, each model applies the same shell (thickness, density) throughout the entire microgel as it is observed for spherical microgels. By subtracting scattering amplitudes of homogeneous particles from one another, the form factor is obtained.

Dubbert et al. reported that due to the synthesis with sacrificial cores, the hollow-shell microgels can have a more complex polymer density profile than that of a model with one shell added to the core.[3] Hence, we decided to start the fitting with a free-form approach using five shells:[4–7] the thickness of the complete shell is fitted and each single shell has the same width (overall shell divided by 5). As fit parameters the heights of each shell (polymer volume fraction) are used.

In Figure S6 (left) the polymer volume fraction profile of the short semi axis (for ellipsoid) and the radius (for cylinder) is shown versus the distance from the center of the microgel. The long semi-axis/half length profile is constructed in the same manner, but with a larger cavity in the center compared to the shown profile. To be able to fit the fuzziness of the inner and outer surface of the entire shell independently from the thickness, a Gaussian with the width of σ_{smear} is used for the surfaces. Using this five-shell model, we identify the shell structure without any prior assumptions and still with a low number of fit parameters. Hence, we get an idea about the polymer profile and also can distinguish if the cylindrical or ellipsoidal shape reproduces the scattering data best keeping in mind that features in the polymer volume fraction can come from the difference in thickness/density of the microgel

shell of the short to the long axis additionally. After the five-shell approach shows the shape and the polymer volume fraction within the microgel, it is determined if it is possible to use the one- (Figure S6 middle) or two- (Figure S6 right) shell models for the density profile of the polymer volume fraction.

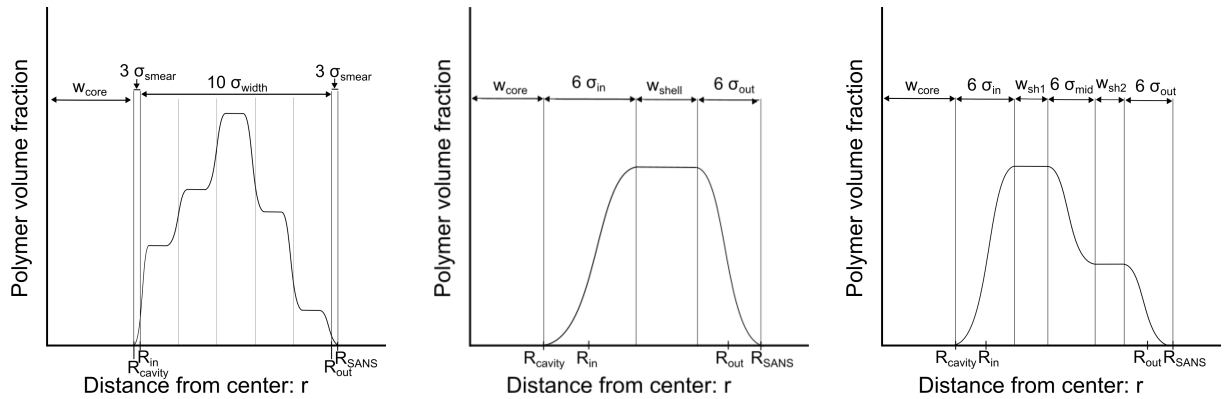

Figure S6: Polymer volume fraction profiles along the short-semi axis/radius for a five- (left), one- (middle) and two- (right) shell model.

The polymer volume fraction profile of the one-shell model is shown in Figure S6 (middle). Similar to the five-shell approach, it consists of a core contribution which has a height set to 0 and a width of the shell with a height different from 0 showing the profile along the short semi axis (for ellipsoid) or the radius (for cylinder). To obtain a fuzzy structure the inner and outer surfaces are defined with a Gaussian of σ_{in} for the width of the inner surface and σ_{out} for the outer surface. The inner and outer radii (R_{in} and R_{out}) are set to the values at half the width of the Gaussian similar to Dubbert et al.[3] For the long semi-axis (ellipsoid) and the half length (cylinder) the same profile is constructed, but with a cavity in the center equal to the long semi-axis/half length of the core.

The two-shell approach consists of similar inner and outer surfaces as in the one-shell approach. Additionally to the one-shell model, this model has two different width for two shells (w_{sh1} and w_{sh2}). Furthermore, both shells are fitted with different amplitudes and are connected with another Gaussian with a width defined by σ_{mid}. In the following, an example of calculating the form factor of the hollow microgel shell for each shape (cylinder ;equation

S1 and ellipsoid; equation S2) are shown. Both examples show the same main structure. The inner cylinder/ellipsoid is subtracted from the outer one:

$$P_{inho.cyl} = L_{out}R_{out}^2 \frac{2J_1(qR_{out}\sin\alpha)}{qR_{out}\sin\alpha}\frac{\sin(qL_{out}\cos\alpha/2)}{qL_{out}\cos\alpha/2}\exp\left(-\frac{\sigma_{out}^2 q^2}{2}\right) - L_{min}R_{in}^2 \frac{2J_1(qR_{in}\sin\alpha)}{qR_{in}\sin\alpha}\frac{\sin(qL_{in}\cos\alpha/2)}{qL_{in}\cos\alpha/2}\exp\left(-\frac{\sigma_{in}^2 q^2}{2}\right) \tag{S1}$$

$$P_{inho.ellip} = \frac{4\pi}{3}R_{out}^3\epsilon_{out}F_1(q, r(R_{out}, \epsilon_{out}, \alpha))\exp\left(-\frac{\sigma_{out}^2 q^2}{2}\right) - \frac{4\pi}{3}R_{in}^3\epsilon_{in}F_1(q, r(R_{in}, \epsilon_{in}, \alpha))\exp\left(-\frac{\sigma_{in}^2 q^2}{2}\right) \tag{S2}$$

where α is the angle between the main axis and the scattering vector. For the isotropically distributed orientations, the expressions have to be integrated over this angle as done in equations 2 and 3 in the main text. Furthermore, the polydispersity of the length and width of either the cylinder or ellipsoid is considered with a normalized Gaussian:[3]

$$D(S, \langle S\rangle = 1, \sigma_{poly}) = \frac{1}{\sqrt{2\pi\sigma_{poly}^2\langle S\rangle^2}} exp\left(-\frac{(S-\langle S\rangle)^2}{2\sigma_{poly}^2\langle S\rangle^2}\right) \tag{S3}$$

with the relative polydispersity (σ_{poly}) and an average scale factor of $\langle S\rangle = 1$.

The instrumental smearing of the SANS data is considered with the resolution function ($Re(\langle q\rangle, q)$),[8,9]

$$Re(\langle q\rangle, q) = \frac{q}{\sigma_{re}^2}\exp\left[-0.5\left(q^2 + \frac{\langle q\rangle^2}{\sigma_{re}^2}\right)\right] I_0\left(\frac{\langle q\rangle q}{\sigma_{re}^2}\right) \tag{S4}$$

where $I_0(x)$ is the modified Bessel function of first kind and zero-order, $\langle q\rangle$ is the nominal scattering vector and σ_{re}^2 is the width of the instrumental resolution/smearing.

The values for the fit parameters of the microgels with the matched silica core (SiM) are listed in table S3 and the values for the hollow microgels (M) in table S4. As the SANS

has no resolution from below 5 nm, such values can be assumed to be 0 (especially for σ) resulting in no meaningful values. Hence, when the fitting procedure showed insignificant values for these parameters, they were fixed to values below 5 nm. We decided to do this as the values are needed to run the fit. The width of the core (w_{core}) and the aspect ratio of the outer shell (ϵ_{out}) have no error as these values are, respectively, fixed at the values for the core according to the results from SAXS, and calculated from the values for the core and the width of the shells, respectively.

Table S3: Fit results for *SiM*.

	T [°C]	ϵ_{out}	w_{core} [nm]	w_{sh1} [nm]	w_{sh2} [nm]	σ_{in}	σ_{mid}	σ_{out}	$\xi_{lor}[nm]$	I_{sh1}	I_{sh2}
SiM76	20	1.73	37.8	0	122 ±18	< 5	< 5	< 5	12.1 ±0.4	1	1
	50	2.10	37.8	30.6 ±1	< 5	< 5	7.2 ±0.2	< 5	-	1	1.76 ±0.04
SiM40	20	1.80	37.8	100 ±6	0	< 5	< 5	< 5	10.0 ±0.3	1	2.3 ±0.6

	T [°C]	ϵ_{out}	w_{core} [nm]	R_{out} [nm]	σ_{smear}	σ_{inner}	ξ_{lor} [nm]	I_{sh1}	I_{sh2}	I_{sh3}	I_{sh4}	I_{sh5}
SiM40	50	2.63	37.8	78.0 ±2	< 5	< 5	-	1	1.5 ±0.2	1.3 ±0.2	0.16 ±0.09	0.48 ±0.09

The fit parameters shown in the Table S3 for the ellipsoidal model are the aspect ratio of the outer shell ($\epsilon_{out} = L_{out}/R_{out}$), the half width of the core (w_{core}), the width of the first (w_{sh1}) and second shell (w_{sh2}). σ_{in} describes the width of the Gaussian between the core and the first shell, σ_{mid} the Gaussian connecting the two shells and σ_{out} the Gaussian representing the fuzzy decay at the outer surface. Note that for this models, σ is added as shown in the sketches of the polymer volume fraction in Figure 2. For example, to obtain the inner radius of the shell (R_{in}) $3\times\sigma_{in}$ is added to the core ($R_{in} = w_{core} + 3\sigma_{in}$). ξ_{lor} defines the mesh-size of the microgel, which is only present in the swollen state as the Lorentzian is not included at high temperatures. I_x gives the intensity of the polymer volume fraction for the shell x. I_{sh1} is fixed at 1 and the other intensities are accounting relative to I_{sh1}.

Table S4: Fit results for M.

	T [°C]	L_{core} [nm]	w_{core} [nm]	w_{sh1} [nm]	w_{sh2} [nm]	σ_{in}	σ_{mid}	σ_{out}	ξ_{lor} [nm]	I_{sh1}	I_{sh2}
M76	20	113 ±17	32 ±7	61 ±8	97 ±8	5.1 ±0.4	7.0 ±0.4	< 5	10.4 ±0.2	1	0.79 ±0.04
	50	110 ±4	38 ±1	3 ±3	0	< 5	10 ±1	< 5	-	1	1.66 ±0.05
M40	20	234 ±3	47 ±1.4	22 ±7	0	< 5	7 ±1	< 5	10.5 ±0.2	1	1.8 ±0.1
	50	135 ±4	10 ±0.2	0	-	8.37 ±0.04	-	< 5	-	1	-

Table S4 shows the fit-parameters used for the cylinder fits. In this case the anisotropy of the model is defined with the length of the core (L_{core}). All other parameters are described above.

The following Figure S7 shows the polymer volume fractions from the short axis of *SiM40/M40* (left) and *SiM76/M76* (right). The colors are chosen to match with the scattering data in the main text. On the left for *SiM40/M40* the blue colors indicate the swollen microgels at 20 °C and the red colors the microgels at 50 °C. The right image corresponding to *SiM76/M76* shows the swollen state (20 °C) in green and the collapsed one (50 °C) in violet. The area of the profiles for each microgel was normalized to the area of the hollow microgels in the collapsed state. This was done because the polymer mass has to be equal in all 4 states of one microgel.

As discussed before, the profiles look more complicated compared with spherical microgels. We do not fully understand these profiles yet and, therefore, avoid any over interpretations. A possible critic assumption is the simplification of adding the same shell at the long and short axis of the microgel. It seems to be that this assumption is much better for the microgel with the thicker shell compared with the thinner one. Even if we cannot exploit these profiles further at the moment and further experiments combined with modeling based on advances computer simulations are required, the main message of this letter, of synthesizing anisotropic hollow microgels, is certain as this model was the easiest model (lowest

number of fit-parameters) usable to fit the scattering data of both microgels and especially the anisotropic shape was additionally confirmed with cryo-TEM.

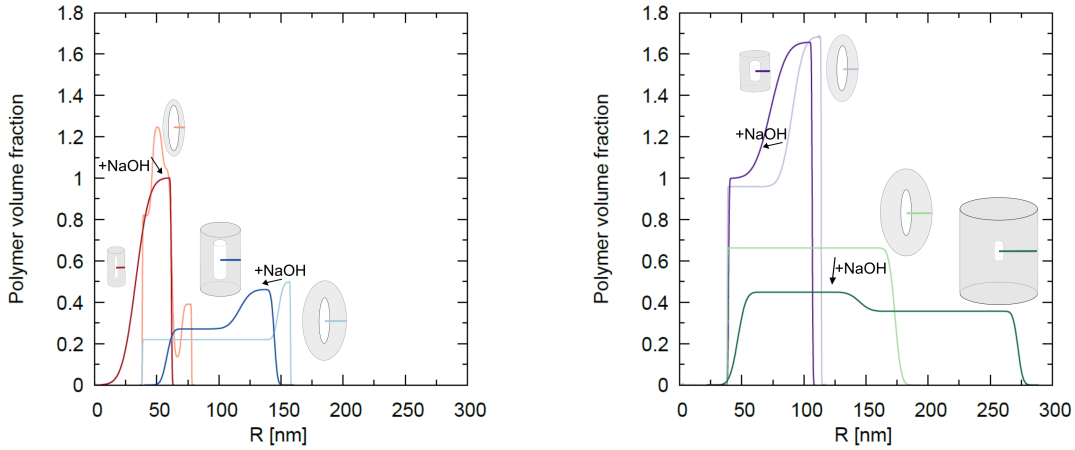

Figure S7: Polymer volume fraction of the microgels *SiM40/M40* (left) and *SiM76/M76* (right) above (50 °C) and below (20 °C) the VPTT and their consequential structure as sketches. In the sketches the horizontal lines show the position of the relative polymer fraction in the microgel structure.

Comparison between fuzzy ellipsoid and fuzzy cylinder models

The microgels without inorganic core (*M40* and *M76*) are fitted with the fuzzy ellipsoid and fuzzy cylinder models. This is done to obtain information on whether the shape of the microgel shell has changed after the etching away of the silica core, which defined the inner shape. The comparison between fits from the fuzzy ellipsoid model (black solid line) and the fuzzy cylinder (solid lines, colors are chosen to match with the ones in the main text) are shown in Figure S8. The first row in Figure S8 are for *M40* and the second one for *M76*, where the left plots correspond to the measurements at 20 °C and the right ones to 50 °C. The scattering data in all four plots and their corresponding fits demonstrate that both models fit the data well. As both models are for anisotropic shapes, this similarity is reasonable. Nevertheless, in each of the four cases the fits resulting from the fuzzy cylinder

model give a lower χ^2 compared to the fuzzy ellipsoid model. Hence, as both models have the same number of fit parameters, the cylinder model is the best suited model to fit the microgel scattering data in the present work, and therefore the results for the sizes of this shape are given. As a conclusion, a small change in the shape is observed after etching away the core for both microgels at both temperatures.

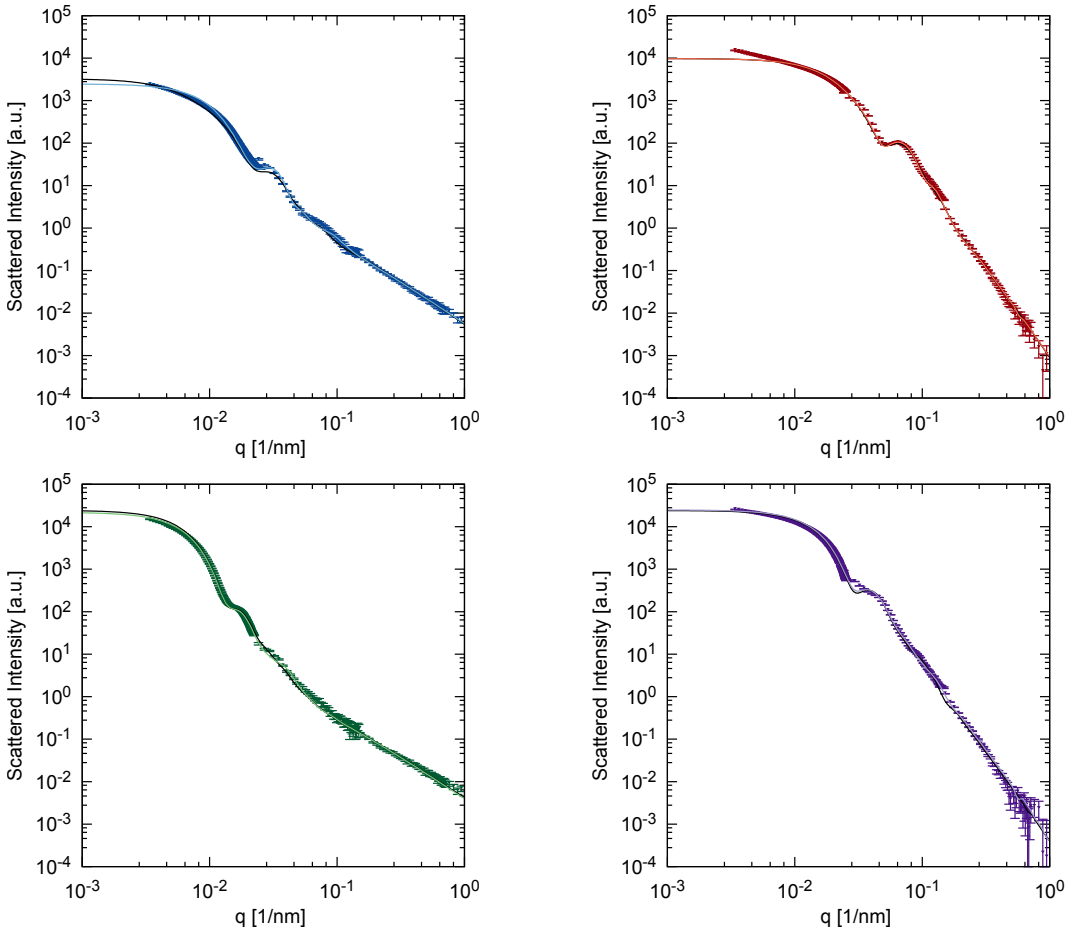

Figure S8: Comparison between ellipsoid and cylinder model fits for *M40* (first row) and *M76* (second row) at 20 °C (left) and 50 °C (right). The ellipsoidal model fits are shown with the black solid line and the cylindrical model fits with the differently coloured solid lines.

References

(1) M. Doucet et al. SasView Version 4.1.2, Zenodo, 10.5281/zenodo.825675.

(2) Virtanen, O. L. J.; Mourran, A.; Pinard, P. T.; Richtering, W. *Soft Matter* **2016**, *12*, 3919–3928.

(3) Dubbert, J.; Honold, T.; Pedersen, J. S.; Radulescu, A.; Drechsler, M.; Karg, M.; Richtering, W. *Macromolecules* **2014**, *47*, 8700–8708.

(4) Pedersen, J. S. *Journal of Applied Crystallography* **1992**, *25*, 129–145.

(5) Pedersen, J. S.; Hamley, I. W. *Journal of Applied Crystallography* **1994**, *27*, 36–49.

(6) Oliveira, C. L. P.; Gerbelli, B. B.; Silva, E. R. T.; Nallet, F.; Navailles, L.; Oliveira, E. A.; Pedersen, J. S. *Journal of Applied Crystallography* **2012**, *45*, 1278–1286.

(7) Keidel, R.; Ghavami, A.; Lugo, D. M.; Lotze, G.; Virtanen, O.; Beumers, P.; Pedersen, J. S.; Bardow, A.; Winkler, R. G.; Richtering, W. *Science Advances* **2018**, *4*, 1–8.

(8) Pedersen, J. S.; Posselt, D.; Mortensen, K. *Journal of Applied Crystallography* **1990**, *23*, 321–333.

(9) Stieger, M.; Richtering, W.; Pedersen, J. S.; Lindner, P. *Journal of Chemical Physics* **2004**, *120*, 6197–6206.